Electrical Power and Energy Systems 155 (2024) 109539

Contents lists available at ScienceDirect

International Journal of Electrical Power and Energy Systems

journal homepage: www.elsevier.com/locate/ijepes

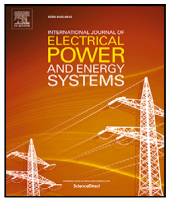

Coordination of distributed resources for frequency support provision in microgrids

Diana Patricia Morán-Río [a,*], Adolfo Anta [b], Javier Roldán-Pérez [a], Milan Prodanović [a], Aurelio García-Cerrada [c]

[a] Electrical Systems Unit, IMDEA Energy, Av. Ramon de La Sagra, 3, Mostoles, 28935, Madrid, Spain
[b] Center of Energy, Austrian Institute of Technology (AIT), Giefinggasse, 4, Vienna, 1210, Austria
[c] Institute for Research in Technology (IIT) ICAI Engineering School, Pontifical Comillas University, Alberto Aguilera, 25, Madrid, 28015, Spain

ARTICLE INFO

Keywords:
Microgrid
Inertia
Grid-forming
Nadir
ROCOF
Small-signal analysis

ABSTRACT

To address the reduction of system inertia, transmission system operators are now requesting converter-interfaced generators (CIGs) to participate in frequency support services. Microgrids (MGs) and virtual power plants have been used as a solution for aggregation of small CIGs. It has been recently considered they may use their combined actions to provide frequency services. However, these proposals are not general enough, focusing on specific CIGs controllers and, in many cases, stability and operational limits are not considered. This paper presents an standardised methodology to design MG controllers that are in compliance with the MG transient response specifications (frequency nadir and rate-of-change-of-frequency, ROCOF). The methodology has an iterative nature and can be applied when the network conditions change. In each iteration, the control parameters are adjusted based on the sensitivity of the system eigenvalues against the frequency metrics of interest while stability and operational constraints are respected. Compared to the literature, the use of quantitative parametric sensitivity is performed for the reallocation of several eigenvalues using two sensitivity components, not only one. Moreover, it is suitable for any combination of grid-forming and grid-following devices. The proposed methodology is applied to a benchmark MG and results show that both nadir and ROCOF can be effectively modified and set as required. The methodology was validated by using a real MG comprising four 15 kW converters and one 75 kW converter.

1. Introduction

1.1. Motivation

The substitution of conventional generation by renewable generation is reducing power system inertia. In response to this situation, many system operators require renewable power plants to participate in frequency-related ancillary services such as fast frequency response and inertia emulation [1–3]. These services are usually aimed at large power plants, which are the common actors in ancillary-service markets. Still, power ratings of distributed generators are significantly lower and, in order for them to participate in these markets, they need to be aggregated first as virtual power plants (VPPs) or microgrids (MGs). However, the frequency response of these aggregations cannot be often predicted. In other words, it is difficult to guarantee the injection of specific power profiles during frequency events and then the participation of these entities in frequency markets is not straightforward. This aspect has attracted the attention of researchers and the concept of dynamic virtual power plant (DVPP) has been proposed to study, among others, the provision of ancillary services by VPPs and MGs [4]. Therefore, the development of methodologies to ensure a specific MG frequency response is of interest.

1.2. State of the art

VPPs and MGs commonly consist of a heterogeneous mixture of grid-forming (GFM) and grid-following (GFL) converters and can, therefore, provide a wide palette of grid services. In the field of inertial services, contributions have focused on the design of grid-forming controllers and the provision of adequate inertial responses. Several authors have proposed the use of dedicated storage devices with a control scheme that emulates some of the characteristics of synchronous machines [5]. Although by using this solution the response can be flexibly adjusted, the need of a dedicated device increases the cost and reduces the feasibility of the solution. Regarding the provision of frequency-support services without storage, the coordination of CIGs using a

* Corresponding author.
E-mail address: dpmoran@comillas.edu (D.P. Morán-Río).

https://doi.org/10.1016/j.ijepes.2023.109539
Received 26 February 2023; Received in revised form 4 August 2023; Accepted 27 September 2023
Available online 18 October 2023

secondary controller was proposed in [6]. However, inertial services must be relatively fast and the response time of centralised controllers usually limit the feasibility of this option. To avoid these limitations, some researchers have proposed methodologies for designing the primary controllers (inherently faster than secondary controllers), such as droops and virtual synchronous machines (VSMs), so they operate as a single device with a customised inertial response [7–11].

In [7], the parameters of several VSMs in a MG are calculated using particle swarm optimisation to guarantee frequency stability against disturbances. In the MG presented in [8], the VSM parameters are adjusted by using a linear quadratic regulator according to frequency disturbances in the grid. In [10,11], analytical aggregated models of VSMs are developed. Taking into account these models, VSM parameters can be adjusted so the aggregated response of all units has specific inertial characteristics. These references focus on external primary controllers (e.g., VSMs), while inner control loops such as virtual impedance and voltage control are sometimes taken into consideration. However, current control loops are commonly neglected [10]. Still, only few authors have studied the coordinated design of droop controllers in MGs for adjusting their inertial response. For example, in [12], the primary controllers of a MG are adjusted to have an aggregated droop characteristic. This is achieved by solving an optimisation problem. On the one hand, analytical methods give a better insight on the impact of parameters on frequency dynamics, however, an analytical study must be carried out to understand the operation of each device. On the other hand, optimisation tools do not require detailed analytical derivations and, therefore, they are simpler to use with a variety of devices. However, these methods do not provide information about the relationship between control parameters and frequency dynamics.

When the operating conditions change, the MG controller parameters may need to be reconfigured to meet the frequency specifications [13]. Examples of when controllers need to be redesigned are: after a generator is connected/disconnected, when power sharing among units changes or when battery droop characteristics are adjusted according to the battery state of charge [14]. Sensitivity analysis has been commonly used for adjusting converter controllers and to study their influence on system eigenvalues (and, therefore, their stability) [15]. Some authors have designed controllers by defining the location of a single eigenvalue, using parametric sensitivity. This has been done by using one [16] or the two [17] components of the sensitivity. However, the use of more than one eigenvalue has not been explored yet.

1.3. Contribution

In this article, a methodology is proposed to re-calculate the control parameters of power converters in MGs in order to adjust their combined frequency response. Then, this methodology is applied to a MG based on a CIGRE benchmark model. The main contributions are summarised in the following list:

- A systematic methodology is proposed to readjust the response of the MG frequency. This methodology is based on the eigenvalue sensitivity and the effect of the control parameters on the center of inertia (COI) frequency. Despite the extensive use of similar tools in the literature, to the authors knowledge, they have not been used to adjust the dynamics of a whole MG.
- Compared to the methods in the literature, the use of quantitative parametric sensitivity is performed for the reallocation of several eigenvalues using two sensitivity components, not only one.
- Parameter constraints resulting from the operating point are taken into consideration during the design procedure. This is another contribution of this work.
- Compared to most of the existing methods in the literature, the proposed methodology is suitable for any combination of GFM and GFL devices.

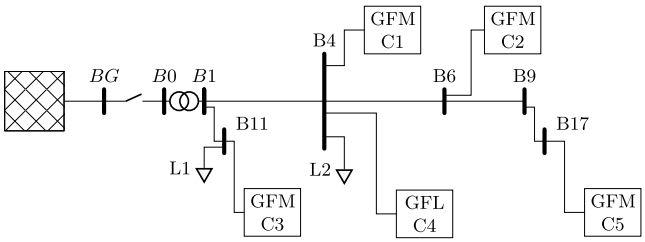

Fig. 1. Single-line diagram of the MG studied in this work.

- Theoretical results are validated experimentally by using a Cigré low-voltage benchmark test network that was adapted to the laboratory facilities.

1.4. Organisation

This paper is organised as follows. The MG topology, the converter controllers and an overview of the proposed methodology are presented in Section 2. Section 3 details the methodology. Implementation is described in Section 4. Experimental results validating the methodology can be found in Section 5 and conclusions are drawn in Section 6.

2. Overview

2.1. Application description

Fig. 1 shows the single line diagram of the MG studied in this work. It is a simplified version of the low-voltage distribution benchmark network for the integration of distributed energy resources (DERs) proposed by Cigré [18]. In this paper, this network is depicted as an islanded MG that can also be connected to the grid and exchange power with it through node $B0$. The system consists of a feeder and a transformer that feeds two resistive loads ($L1$ and $L2$). DERs such as PV, wind generation and storage may be interfaced by means of a GFL converter ($C4$) or by a GFM converter ($C1, C2, C3$ and $C5$). All the converters have an LCL filter.

2.2. Control overview

The GFL converter controls the active and reactive power injected to the grid. For that purpose, it has a PI controller that regulates the current through the converter-side inductance of the LCL filter. A phase-locked loop (PLL) is used to synchronise the converter with the voltage of its connection point.

GFM devices (see Fig. 2) are equipped with an inner current loop and an outer voltage loop. The current loop is used to regulate the current through the converter-side inductance ($\vec{i}_i(t)$). The arrow over the variable name indicates that the signal is in a dq reference frame (e.g., $\vec{i}_i(t) = i_{i-d}(t) + j i_{i-q}(t)$) and j is the imaginary unit. The time dependence of signals will be dropped from now on for the sake of clarity. This current controller is based on a PI controller applied over the current error, in dq. It also includes standard decoupling terms. The current error is defined as follows [19]:

$$\vec{\epsilon}_i = \vec{i}_i^* - \vec{i}_i, \tag{1}$$

where the asterisk "$*$" stands for "reference". A voltage controller is used to regulate the voltage across the ac capacitor $\vec{v}_c$. It is also based on a PI controller applied over the voltage error, where the effect of the virtual impedance is also included [19]:

$$\vec{\epsilon}_v = E - \vec{v}_c - \vec{v}_v, \tag{2}$$

where E is the voltage reference and $\vec{v}_v$ is the voltage generated by the virtual impedance. This controller also includes standard decoupling terms [19].

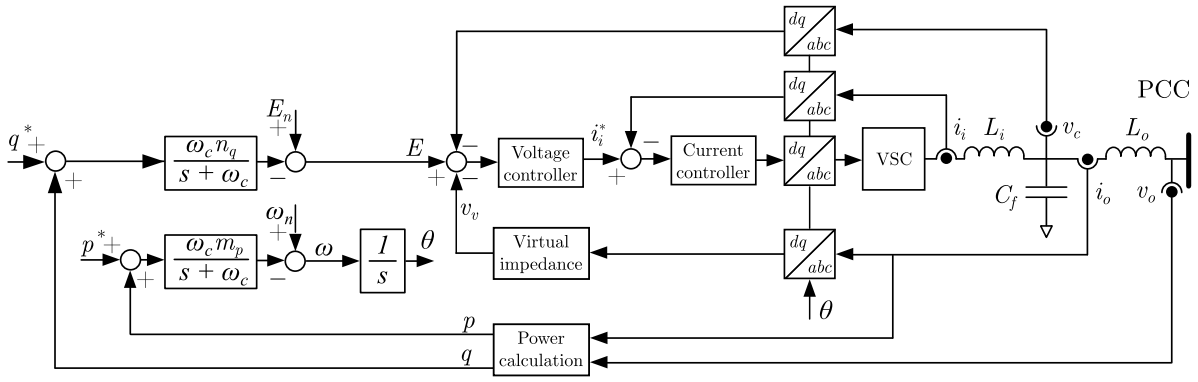

Fig. 2. Electrical and control system diagram of a grid-forming converter.

A quasi-stationary virtual impedance is applied on top of the voltage controller. This virtual impedance facilitates the connection of GFM devices in parallel configuration (i.e., when forming a MG) [20]:

$$\vec{v}_v = -(j\omega L_v + R_v)\vec{i}_o, \tag{3}$$

where L_v and R_v are the inductive and resistive parts of the virtual impedance, ω is the frequency generated by the droop control and $\vec{i}_o$ is the output current.

The frequency and voltage magnitude control references are internally generated according to [21]:

$$\omega(s) = g_1(P(s), Q(s)), \quad E(s) = g_2(P(s), Q(s)), \tag{4}$$

where s stands for the Laplace variable, ω represents the frequency, E the voltage magnitude, $P(s)$ and $Q(s)$ the measured active and reactive power, and $g_1(\cdot)$ and $g_2(\cdot)$ are the desired GFM characteristics. In low-voltage grids, the grid frequency affects the voltage regulation while the reactive power takes part in MG frequency regulation [22]. Therefore, in order to use traditional droops, the output inductance of the converter is commonly increased [23]. In this paper, this is achieved by combining the effect of output inductance of the LCL filter plus a virtual impedance loop. Since virtual and coupling impedances are implemented here, conventional frequency and voltage droops are considered in this work, although other options could be also implemented [15]:

$$\omega(s) = \omega_n - m_p\tilde{P}(s), \quad E(s) = E_n - n_q\tilde{Q}(s), \tag{5}$$

where ω_n and E_n are the no-load frequency and voltage magnitudes, and m_p and n_q are the droop characteristics. $\tilde{P}(s)$ and $\tilde{Q}(s)$ are the filtered active and reactive powers injected by the unit [15]:

$$\tilde{P}(s) = \frac{1}{s/\omega_c + 1}P(s), \quad \tilde{Q}(s) = \frac{1}{s/\omega_c + 1}Q(s), \tag{6}$$

where ω_c is the cut-off frequency of the filter. The equivalent inertia (H_i), measured in seconds (s), of the ith GFM converter can be calculated as [24]:

$$2H_i = \frac{1}{\omega'_{ci}m'_{pi}} \tag{7}$$

being ω'_{ci} and m'_{pi} the pu values of the cut-off frequency and constant of the droop controller.

2.3. Methodology overview

The aim of the proposed methodology is to redesign the controllers of a MG to achieve some specific metrics. In this work, metrics related to the transient response of the frequency of the MG COI have been chosen. However, the proposed methodology is generic enough and can be also adapted to adjust other ones.

For simplicity, in this work the frequency of COI is used as a measurement of the whole MG frequency. Borrowing the notion from conventional power systems, the COI frequency is defined as follows [25,26]:

$$\omega_{COI} = \frac{\sum_{i=1}^{n}\omega_i H_i}{\sum_{i=1}^{n} H_i}, \tag{8}$$

where ω_i is the frequency of the ith converter. The desired transient response is designed by defining the nadir and/or the rate-of-change-of-frequency (ROCOF), and it is applied by changing the DER primary controller configuration.

Fig. 3 shows the flowchart of the proposed methodology. The relations between nadir, ROCOF and the control parameters are determined by using the MG small-signal model, parametric sensitivities and participation factors. Then, the parameters are modified based on these relations. The new control parameters are validated according to the stability and operational constraints. Since the methodology is based on the use of linear tools, the MG control parameters should be modified by using small increments to prevent any drifting from the original operating point. After an iterative search, the definitive values of the parameters are selected. In addition, as the system eigenvalues are placed far away from the imaginary axis during the iterative process, the system would be relatively robust against the changes of the operating point.

3. Methodology

In this section, the proposed methodology is explained. First, small-signal tools are described. Then, the relations between COI dynamics, system eigenvalues and control parameters are derived. Finally, the iterative search for the control parameters is explained. Unless otherwise specified, the expressions in this section are presented in time domain.

3.1. Small-signal modelling of the MG

A small-signal model of the MG can be described in the time domain as follows [27]:

$$\begin{aligned}\left[\Delta\dot{x}\right] &= A\left[\Delta x\right] + B\left[\Delta u\right],\\ \left[\Delta y\right] &= C\left[\Delta x\right] + D\left[\Delta u\right],\end{aligned} \tag{9}$$

where Δx is the state vector, Δu is the input vector, Δy is the output vector A, B, C and D are the state-space matrices. The state-space model is derived considering a power variation in the load (ΔP_L) as the input and $\Delta\omega_{COI}$ as the output, following the methodology presented in [15]. The transfer function from a load step to ω_{COI} is used to study frequency dynamics.

In the following subsections, the models of the MG elements are briefly explained. Nonetheless, the exact models and the details can be found in [15,19]

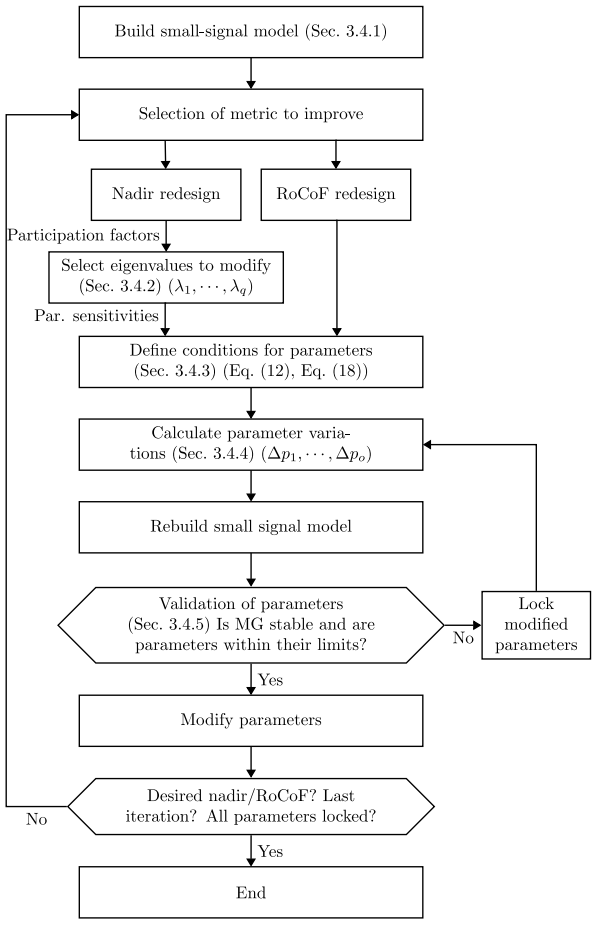

Fig. 3. Flowchart diagram of the proposed methodology.

3.1.1. Modelling of GFM converters

The model of GFM converters includes the description of the LCL filter and all the control loops described in Section 2.2. Then, the equations of the converter are linearised, following the procedure described in [15]. The state vector of each GFM converter is as follows:

$$x_{GFM} = [i_{i-d} \;\; i_{i-q} \;\; v_{c-d} \;\; v_{c-q} \;\; i_{o-d} \;\; i_{o-q} \;\; \gamma_d \;\; \gamma_q \;\; \phi_d \;\; \phi_q \;\; \tilde{p} \;\; \tilde{q} \;\; \delta]', \tag{10}$$

where $\vec{\gamma}$ are the states of the current PI controller, $\vec{\phi}$ are the states of the voltage PI controller, δ is the angle of the droop control, and $\tilde{p}$ and $\tilde{q}$ are the states of the filtered active and reactive powers, respectively.

3.1.2. Modelling of GFL converters

Each GFL converter includes a current controller with decoupling terms and a standard PLL. The state-vector of each GFL converter is as follows:

$$x_{GFL} = [i_{i-d} \;\; i_{i-q} \;\; v_{c-d} \;\; v_{c-q} \;\; i_{o-d} \;\; i_{o-q} \;\; \gamma_d \;\; \gamma_q \;\; \delta_{PLL}]', \tag{11}$$

where δ_{PLL} is the angle generated by the PLL.

3.1.3. Modelling of loads and lines

Loads are modelled with a series-connected LR equivalent circuit. Electrical lines are also modelling by using a LR equivalent. Therefore, each line and load add two state variables (one for the d component of the current, and another one for the q component). See [15] for more details.

3.1.4. Aggregate model of the MG

All the linearised state-space models of the GFM converters, the GFL converters, the lines and the loads are merged together in a single state-space representation, following the procedure presented in [15]. This model is linear, although its parameters depend on the system operating point. Therefore, for an accurate representation, the state-space model should be recalculated according to the operating point.

3.2. Participation factor analysis

In this work, the MG stability have been studied by using the system eigenvalues as these are a global measure of stability [28]. Other open- and closed-loop techniques may also be used to analyse stability [27]. This has not been explored here, but it might be of interest for further research.

The participation matrix (P_M) establishes the link between state variables in (9) and eigenvalues of A [28]:

$$P_M = \begin{bmatrix} f_{11} & \cdots & f_{1m} \\ \vdots & \ddots & \vdots \\ f_{m1} & \cdots & f_{mm} \end{bmatrix}, \quad f_{ki} = \frac{\partial \lambda_i}{\partial a_{kk}} = \psi_{ik}\phi_{ki}, \tag{12}$$

where the participation factor f_{ki} measures the participation of the ith eigenvalue (λ_i) on the kth state variable (Δx_k), m denotes the number of states, and ψ and ϕ are the left and right eigenvectors associated with λ_i. In order to study the dynamics of $\Delta\omega_{COI}$, the output $\Delta\omega_{COI}$ has been described as a function of the state variables and the inputs using (8) and (9):

$$[\Delta\omega_{COI}] = C_{COI}\,[\Delta x] + D_{COI}\,[\Delta u], \tag{13}$$

where the first term fully defines $\Delta\omega_{COI}$, so $D_{COI} = 0$. The participation vector of $\Delta\omega_{COI}$ shows which eigenvalues participate more in $\Delta\omega_{COI}$ and can be simply calculated as:

$$P_{COI} = C_{COI} P_M. \tag{14}$$

3.3. Eigenvalue sensitivities

In this work, the eigenvalue sensitivities are used to understand how each control parameter participates in the dynamics of $\Delta\omega_{COI}$. Parametric eigenvalue sensitivities are defined as the derivative of a system eigenvalue with respect to a parameter [16,28,29]:

$$s_{ij} = \frac{\partial \lambda_i}{\partial p_j} = \psi_i \frac{\partial A}{\partial p_j} \phi_i, \tag{15}$$

where s_{ij} is the sensitivity of eigenvalue λ_i with respect to parameter p_j, ψ_i and ϕ_i are the left-row eigenvector and the right-column eigenvector associated to λ_i, respectively. Sensitivities are complex numbers that describe, in a quantitative manner, how eigenvalues move in the complex plane when a parameter is modified.

For small parameter p_j (Δp_j) variations, (15) can be expressed as:

$$\Delta\lambda_i = \lambda_i' - \lambda_i \approx s_{ij}\Delta p_j, \quad \lambda_i' \approx \lambda_i + s_{ij}\Delta p_j, \tag{16}$$

where λ_i' is the value of λ_i after applying Δp_j. This can be extended for variations of o parameters and q eigenvalues:

$$\begin{bmatrix} \Delta\lambda_1 \\ \vdots \\ \Delta\lambda_q \end{bmatrix} \approx \begin{bmatrix} s_{11} \\ \vdots \\ s_{q1} \end{bmatrix} \Delta p_1 + \cdots + \begin{bmatrix} s_{1o} \\ \vdots \\ s_{qo} \end{bmatrix} \Delta p_o. \tag{17}$$

One should notice that (17) is a complex expression and hence a system of $2q$ linear equations if all λ_i are complex. As it will be shown in Section 4.2.3, real and imaginary components of sensitivities have comparable magnitude for the case studied in this work. Therefore, both components will be used to calculate the parameter variations. Other works only use the real components when obtaining their results [16]. However, the validity of this simplification depends on each specific application.

For a given operating point (with its specific eigenvalues and set of parametric sensitivities) the parameter variations that move eigenvalues $\lambda_1, \ldots, \lambda_q$ to their desired location $\lambda'_1, \ldots, \lambda'_q$ can be calculated by solving (17). Since (17) is only valid for small changes in Δp_j, this expression can only be used for small displacements of the eigenvalues. To calculate larger displacements, (17) can be applied iteratively until a solution is found.

3.4. Adjustment of Nadir and ROCOF of $\Delta\omega_{COI}$

3.4.1. Nadir

The transfer function of interest, representing the frequency dynamics, can be written as the sum of the contribution of each eigenvalue weighted by its corresponding residue [28]:

$$G(s) = \sum_{i=1}^{m} \frac{R_i}{s - \lambda_i}, \tag{18}$$

where R_i is the residue of $G(s)$ for λ_i. Both participation factors and residues establish the relations between eigenvalues and $\Delta\omega_{COI}$ (see [29] for more details).

Both real and complex eigenvalue dynamics are studied here to understand their differences:

- *Effect of One Real Eigenvalue:* When the response of ω_{COI} is dominated by a real eigenvalue, the nadir is approximately $\Delta\omega_{COI}(\infty)$ and can be calculated by applying the final value theorem [27]:

$$\Delta\omega_{COI}(\infty) = \lim_{s\to 0} sG(s)U(s) = \\ = \lim_{s\to 0} G(s) \approx \lim_{s\to 0} \frac{R_i}{s - \lambda_i} = \frac{R_i}{-\lambda_i}. \tag{19}$$

  Therefore, to reduce the nadir in this case, the value of λ_i should be increased, that is, the eigenvalue should be moved to the left. This case is not very representative of a real system with machines, but it can happen in systems with power converters. In this case, the steady-state droop characteristic is directly related to the frequency nadir.
- *Effect of a Pair of Complex Eigenvalues:* In this case, the frequency nadir is linked to the maximum overshoot of the second order system defined by the pair of complex eigenvalues, which is calculated as [27]:

$$\omega_{nadir} = \omega(0) - \Delta\omega_{COI}(\infty)e^{-\pi \tan\alpha}, \tag{20}$$

  where $\omega(0)$ is the frequency before the load variation and $\alpha = \arg(\lambda_i) - \pi/2$. Here, to reduce the nadir, α should increase (i.e., λ_i should be more damped). This case is quite common in conventional power systems applications.
- ***Application to the General Case:*** In a general case where both real and complex eigenvalues participate in $\Delta\omega_{COI}$, it is desired to move real eigenvalues to the left and damp complex conjugated eigenvalues to reduce the nadir.

3.4.2. ROCOF

Qualitatively speaking, lower values of ROCOF can be obtained if the converter controllers react faster to frequency deviations, thereby providing a larger synthetic inertial response. However, the effect of control parameters on the ROCOF cannot be simply derived from eigenvalues (as in the case of the nadir). To understand the effect of the control parameters on the ROCOF, the ROCOF expression has been rewritten in terms of the droop control parameters, as in (7). This representation of the ROCOF is equivalent to its standard definition, but adapted for power converters [24,30]:

$$ROCOF = \frac{\Delta P_{Loss}\Omega_r}{2\sum_{i=1}^{n} S_i H_i} = \frac{\Delta P_{Loss}}{\sum_{i=1}^{n} \frac{1}{\omega_{ci} m_{pi}}}, \tag{21}$$

where ΔP_{Loss} is the power variation in the system that caused the frequency excursion, the denominator represents the kinetic energy of the system and n is the number of droop-controlled converters. In order to obtain an expression that considers parameter variations as variables like (17), in this paper the ROCOF is presented as follows:

$$ROCOF = \frac{\Delta P_{Loss}}{\sum_{i=1}^{n} \frac{1}{\omega_{ci} m_{pi}}} = \frac{\Delta P_{Loss}}{\sum_{i=1}^{n} \frac{1}{\omega_{ci0} m_{pi0}}} \frac{1}{b}, \tag{22}$$

where ω_{ci}, m_{pi} correspond to the new droop parameters, ω_{ci0} and m_{pi0} correspond to the initial ones and b measures the change in the equivalent system inertia. Expression (22) is linearised around the operating point to find a linear relation between the new and the initial droop parameters. After the linearisation, the following expression is obtained:

$$Kb = \left[\Delta\omega_{c1}, \cdots, \Delta\omega_{ci}\right] \begin{bmatrix} \frac{K_1}{\omega_{c10}} \\ \vdots \\ \frac{K_i}{\omega_{ci0}} \end{bmatrix} + \left[\Delta m_{p1}, \cdots, \Delta m_{pi}\right] \begin{bmatrix} \frac{K_1}{m_{p10}} \\ \vdots \\ \frac{K_i}{m_{pi0}} \end{bmatrix}. \tag{23}$$

$$K_i = \frac{1}{\omega_{ci0} m_{pi0}}, \quad K = \sum_{i=1}^{n} K_i. \tag{24}$$

This equation is linear and represents how small changes of the droop parameters affect the ROCOF by means of b. It can be used similarly in (17) to calculate control parameters.

3.5. Iterative search of the solution

When the MG power sharing conditions change, controller parameters need to be redesigned to preserve the same frequency dynamics. The proposed iterative methodology is then applied to redesign the controllers. The iterative search combines all the tools presented above. It is worth noting that the tools described above are widely used in the literature. The specific contribution of the paper is in the proposed methodology that combines all of them in order to control and set the dynamics of the MG. Nonetheless, Eqs. (14) and (23) have been specially derived for that purpose. A flowchart of the methodology is shown in Fig. 3. It has to two main branches, one for setting the ROCOF and another one for setting the nadir. The steps are described in the following text.

3.5.1. Small-signal modelling

In this step, the small-signal model of the MG is derived analytically [15,19]. Since the parameter adjustment of primary controllers to provide inertia is performed by the MG operator, it is reasonable to assume the device characteristics data and the MG operating point are available for the parameter calculation. Its operating point is calculated using a *Matlab-Simulink* model (alternative options for performing this task can be found in [31,32]).

3.5.2. Selection of target eigenvalues

To adjust the nadir, the eigenvalues that define the transient of ω_{COI} should be modified, that is, the eigenvalues that participate more in ω_{COI}. To this end, the participation factors of ω_{COI} (P_{COI}) are calculated and normalised so that $\sum P_{COI} = 1$. Then, the eigenvalues with the most relevant impact on ω_{COI} (highest participation) are selected. Eigenvalues with a low damping factor are also selected in order to reduce the nadir as indicated in Section 3.4.1.

3.5.3. Definition of parameter conditions

Eqs. (17) and (23) are used to modify the nadir and ROCOF, respectively. Sensitivities and the values of K and K_i (see (23)) are calculated in each iteration since they change with the operating point. For simplifying calculations, sensitivities $\partial A/\partial p_j$ in (15) are calculated as $\Delta A/\Delta p_j$. Additional linear equations may be used to guarantee that certain parameters are modified simultaneously. For instance, in order to keep the same power sharing, the ratios between converter droops (m_{pi}) should be maintained (this will be explained later in more detail).

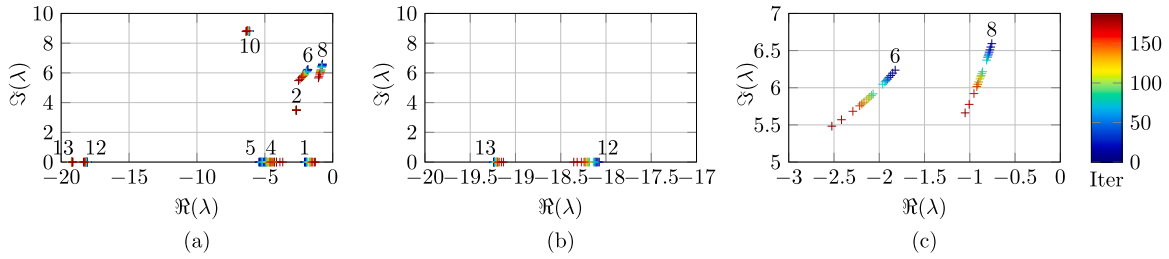

Fig. 4. Eigenvalue loci for *SC2* along the iterations when the nadir is reduced. (a) low frequency eigenvalues. (b) zoom in eigenvalues λ_{12} and λ_{13}. (c) zoom in eigenvalues λ_6 and λ_8.

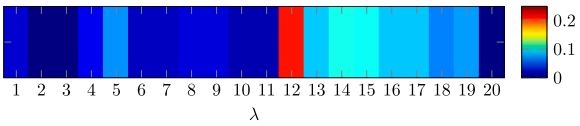

Fig. 5. Eigenvalue participation on ω_{COI} in *SC2*.

3.5.4. Calculation of parameter variations

In general, the number of variables to be calculated, which is the number of variables in (17) (or the number of variables in (23) for a design based on the ROCOF), will be larger than the number of equations. This means that the system will be underdetermined. To minimise the number of control parameters to be modified, the solution that minimises the least-square of Δp_j will be selected [33,34]. Also, since linearised models are used, only small variations of the control parameters will be taken into consideration.

3.5.5. Parameter validation

After calculating the parameter variations, it must be verified that the system remains stable and that parameters remain within their technical limits. If the system is not stable, all parameters that were modified are fixed to their last feasible values. At this point, control parameter constraints may be introduced, for instance in primary controllers to guarantee sufficient bandwidth separation, to limit droop constants and restrict ω_{ci} range, among others. Constraints should be added to the original linear problem, although this would lead to a more complex formulation. Also, if one or more parameters are out of their permitted range, those parameters are fixed to their last feasible value.

3.5.6. Iterating condition

After updating the parameters, the algorithm must check whether the design goal (nadir or ROCOF) has been reached. This is done taking into consideration the new parameters in the small-signal model. As the variations of the parameters must be kept small, several iterations will be required until the solution is reached. Finally, the iterative process stops if the nadir or the ROCOF reach their desired value, if there are no parameters that can be modified, or if the maximum number of iterations is reached.

4. Numerical results

4.1. Case study

The proposed methodology was applied to the MG shown in Fig. 1. The system parameters from the Cigré MG [18] were adapted to the lab facilities, resulting in the line and load parameter values provided in Table 1. The nominal apparent power of converters is 75 kVA for $C1$ and 15 kVA for the rest of them. The power reference of the GFL converter is 1 kW. Unless otherwise stated, current and voltage controllers of GFL and GFM converters have been designed with bandwidths of 250 Hz and 30 Hz, respectively. The PLL has a bandwidth of 1 Hz.

Table 1
Line and load parameters.

Line/Load	Nodes	R [Ω]	L [mH]
Line 1	B4-B6	0.075	0.3
Line 2	B6-B17	0.3	0.1
Line 3	B11-B4	1.075	0.3
Load 1	B11	17.78	–
Load 2	B4	26.67	–

Table 2
Definition of droop parameters and scenarios.

Conv.	Par.	SC1	SC2
$C1$	m_p (%)	0.25% (75 kW)	0.5% (75 kW)
	ω_c	5 Hz	5 Hz
$C2$	m_p (%)	0.5% (15 kW)	0.5% (15 kW)
	ω_c	3 Hz	3 Hz
$C3$	m_p (%)	0.5% (15 kW)	0.5% (15 kW)
	ω_c	5 Hz	5 Hz
$C5$	m_p (%)	0.5% (15 kW)	0.5% (15 kW)
	ω_c	5 Hz	5 Hz

Virtual impedances of 1 Ω and 10 mH were used to allow the parallel operation of GFM converters. The reactive power droop constants were adjusted to allow 2.5% of voltage variation with an injection of the rated power. The low pass filters of the reactive power loops were designed so that they have the same cutoff frequency of those used for active power. The two different scenarios that will be considered in this paper are shown in Table 2, as well as the corresponding droop parameters of the active power controller. A load step change was applied to $L2$ to study the frequency dynamics of the MG.

As a demonstration, the methodology is applied to a case when a change of the power sharing between units is required while retaining certain frequency characteristics at the same time. Initially, MG controllers are designed as in scenario *SC1*. In this scenario, ω_{COI} exhibits the desired nadir and ROCOF. After a certain event, the power sharing between the units is readjusted and m_{pC1} is set to 5 %. Since m_{pC1} is increased, in this new scenario (*SC2*), ω_{COI} features larger nadir and ROCOF compared to *SC1*. Considering the new conditions, that is, new power-sharing ratios between the units, the proposed methodology is applied to set the nadir and the ROCOF to their previous values. The application of the proposed methodology for *SC2* is explained in detail in the following section, where the nadir will be adjusted. The modifications required to adjust the ROCOF will also be explained there. This demonstration case has been defined to show how to include additional restrictions (while retaining the power sharing) in the methodology and to show their impact.

4.2. Application of the proposed methodology

Firstly, the small-signal model of the MG at a general operating point, has been derived analytically.

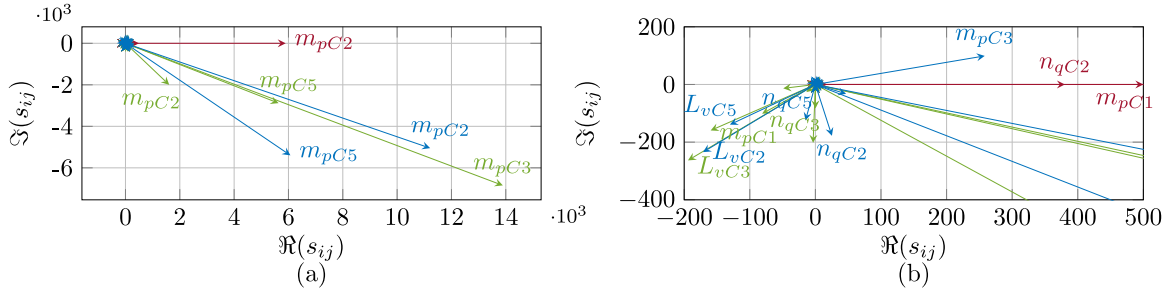

Fig. 6. Parametric sensitivities expressed as vectors of (red) λ_{12}, (green) λ_6 and (blue) λ_8, in *SC2* at the first iteration. (a) Parameters with the highest impact and (b) other parameters with high impact on λ_{12}, λ_6 and λ_8. (For interpretation of the references to colour in this figure legend, the reader is referred to the web version of this article.)

4.2.1. Selection of eigenvalues to modify

The participation factors of ω_{COI} are calculated by applying (14). For example, Fig. 5 shows their magnitude for *SC2*. Only the participation of the low-frequency eigenvalues is shown (lower than 7 Hz). As it can be seen, λ_{12} predominantly participates in ω_{COI}. To reduce the nadir, damping of poorly damped eigenvalues must be improved and real eigenvalues must be moved to the left. Fig. 4(a) shows that the eigenvalues with lowest damping ($\zeta < 0,5$) are λ_6 and λ_8, and their conjugates. Therefore, the objective is to damp λ_6 and λ_8 and move λ_{12} to the left.

4.2.2. Definition of parameter conditions

At this stage, (17) is used. The desired λ'_{12}, λ'_6, λ'_8 are defined to have 1 % higher natural frequency and damping (if complex) than actual λ_{12}, λ_6, λ_8. Furthermore, to keep the same power-sharing ratios between units, the following additional conditions are applied:

$$\begin{aligned} 5\Delta m_{pC1} - \Delta m_{pC2} &= 0, \\ 5\Delta m_{pC1} - \Delta m_{pC3} &= 0, \\ 5\Delta m_{pC1} - \Delta m_{pC5} &= 0. \end{aligned} \tag{25}$$

By adding this condition, the ratio between the absolute droop coefficients is 5 despite the ratings of the units. In the case of ROCOF redesign, (23) must be applied considering the droop parameters and a value of b larger than 1 to reduce the ROCOF with each iteration. Since (23) represents a single equation, the least-square solution of (23) and (25) identifies the four droop parameters to modify. The parameter variations are calculated as detailed below.

4.2.3. Calculation of parameter variations

Now, (17) and (25) are solved. Fig. 6 shows the sensitivities of λ_{12}, λ_6 and λ_8 to droop (m_p, ω_c and n_q), virtual impedance (R_v and L_v), voltage controller (k_{pv} and k_{iv}) and current controller parameters (k_{pc} and k_{ic}). The parameters with highest impact on the considered eigenvalues are droop and virtual impedance parameters. In some cases eigenvalues were also sensitive, to a lesser extent, to voltage-controller parameters but eigenvalues were not sensitive to current-controller parameters. Since the solution of (17) and (25) with the minimum norm is used, eigenvalues are relocated by modifying only droop and virtual impedance parameters (see Fig. 7). When the objective is to modify the ROCOF, (23) and (25) are solved and the four droop parameters are modified in each iteration. After the solution of (17) (or (23)) and (25) is found ($\Delta p_1, \ldots, \Delta p_o$), the new parameter values (p'_j) are calculated. A maximum variation of 1 % was considered to ensure the validity of the displacement prediction made by the sensitivities [16]. Firstly, per unit variations are calculated as $\Delta pu_j = \Delta p_j / p_j$. Then, the largest per unit variation ($\Delta pu_{max} = max(|\Delta pu_j|)$) is computed and it is assigned a variation of 1 % to that parameter. Finally, the values of all other parameters are calculated as follows:

$$p'_j = p_j \left(1 + \text{sign}(\Delta p_j) \frac{1}{100} \frac{|\Delta pu_j|}{\Delta pu_{max}}\right) \tag{26}$$

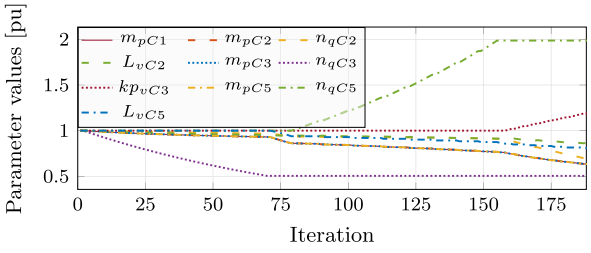

Fig. 7. Per unit parameter values in *SC2* when the objective is to reduce the nadir.

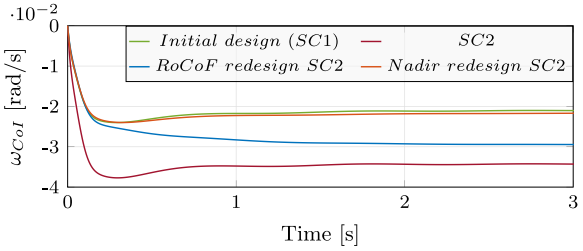

Fig. 8. Transient response of ω_{COI} when there is variation of load L2. (green) Initial design of controllers in *SC1*. Results (red) with battery droop constrains applied (*SC2*), (blue) after modifying parameters to adjust ROCOF in *SC2* and (orange) after modifying parameters to adjust nadir in *SC2*. (For interpretation of the references to colour in this figure legend, the reader is referred to the web version of this article.)

where p'_j denotes the new value for the current iteration of p_j and $|\Delta pu_j|$ is the modulus of the per unit variation of parameter p_j. Fig. 7 shows the per unit parameter values (referred to the initial value) along the iterations for the studied case. The parameters that have been modified to change the nadir are m_{pC1}, m_{pC2}, m_{pC3}, m_{pC5}, n_{qC2}, n_{qC3}, n_{qC5}, L_{vC2}, L_{vC5} and kp_{vC3}. These were the parameters that affected λ_{12}, λ_6 and λ_8 the most, as shown in Fig. 6. Since (17) and (25) sum $5 + 3$ equations altogether, 8 parameters are modified at a time. The values of the target parameters in each iteration are shown in Fig. 7.

4.2.4. Parameter validation

After calculating the new values of the parameters in each iteration, they are validated. If any of the parameters reaches its limit or if the MG becomes unstable for the new configuration, the parameter is blocked. For example, in Fig. 7, when n_{qC3} reaches its lower limit at iteration number 70, it is fixed at its limit. From then on, the nadir is adjusted by modifying n_{qC5}, which had not been modified yet. Similarly, at iteration number 155 n_{qC5} hits its upper limit and kp_{vC3} is modified from then on.

4.2.5. Iterative process

After modifying the parameters, the small-signal model is recalculated to check if the design goals had been achieved. The process

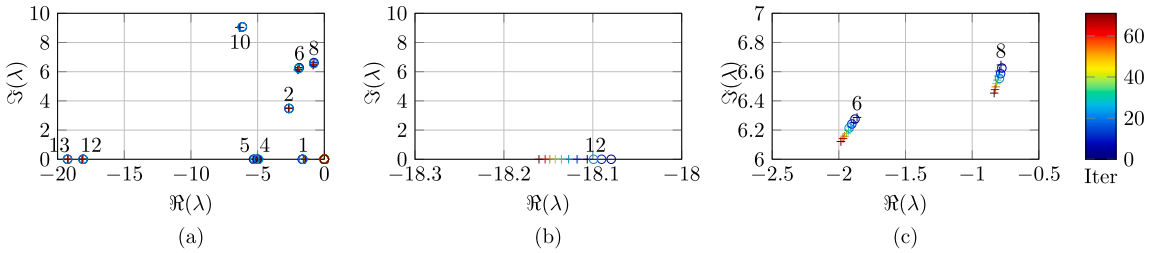

Fig. 9. System eigenvalues of the MG for SC1, when load $\cos\phi = 0.8$ (o) and load $\cos\phi = 1$ (+).

described above is repeated until frequency dynamics metrics reach the desired value and while there are available parameters to be modified. In order to avoid a long iterative process when many parameters are blocked, the maximum number of iterations was set to 500. It was observed that the number of iterations to reach the desired nadir increases with the number of equations to solve. Therefore, it is recommended to avoid modifying too many eigenvalues.

4.3. Simulation results

Fig. 8 shows the transient response of ω_{COI} for $SC1$ and $SC2$, before and after recalculating the control parameters. For obtaining this response, the load $L2$ was increased by 3 kW. Fig. 8 shows that ω_{COI} features larger nadir and ROCOF in *SC2* (in red) compared to *SC1* (in green). After recalculating the controller parameters for adjusting the nadir (in orange), the nadir of ω_{COI} is the same as it was for *SC1*. This is mainly because of the change of the steady state frequency, caused by the changes of droop parameters (m_{pi}). These were the parameters with most significant impact on the selected eigenvalues. Fig. 6 shows the polar representation of the parametric sensitivities of λ_{12}, λ_6 and λ_8. The direction of sensitivities is not the same as the desired direction of movement of eigenvalues. Therefore, a combination of parameter variations is needed to move these eigenvalues. All this information is already taken into consideration in (17). Fig. 4(b) and (c) show that λ_{12} moves to the left and that λ_6 and λ_8 become more damped in each iteration. As a consequence, the nadir is reduced. Incidentally, after the parameter variations, other eigenvalues (apart from λ_{12}, λ_6 and λ_8) also move. Even though these eigenvalues have low participation in ω_{COI}, they may become unstable. Therefore, a minimum damping for all eigenvalues must be enforced. Furthermore, the power-sharing ratio between units is maintained constant along iterations since condition (25) is considered. This is shown in Fig. 7. The per unit variation of m_p is the same for all the GFM units. In this example, adding power sharing restriction (25) produces an easier problem to solve with less degrees of freedom. However, it must be noted that this is not the general case.

Fig. 8 (blue) shows that the ROCOF of ω_{COI} (at $t = 0.1$ s) after redesign takes the original value of *SC1*. Since (23) and (25) sum $1 + 3$ equations, 4 parameters are changed in each iteration. Initially, m_{pC1} is reduced to increase the virtual inertia and (25) ensures that all the droops are modified simultaneously to keep the same power-sharing ratio. Notice that the reference frequency metrics might not be achievable with a feasible set of parameters. In that case, the methodology will stop looking for a solution.

4.3.1. Effect of inductive loads

An additional test was conducted in order to test the algorithm under different types of loads. It was assumed, in particular, that all the loads in the system had an inductive part with $\cos\phi = 0.8$ in SC1 (instead of $\cos\phi = 1$). Then, the algorithm was executed and the objective was to set the nadir at 0.21 Hz. Fig. 9 shows the movement of the eigenvalues for $\cos\phi = 0.8$, marked with "o", and for $\cos\phi = 1$, marked with "+". It can be seen that for the scenario with $\cos\phi = 0.8$,

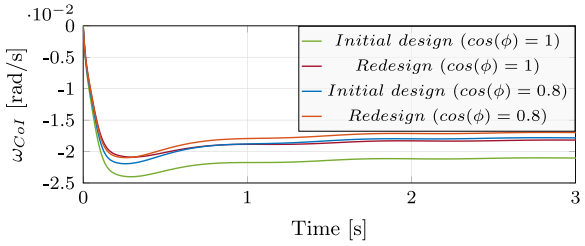

Fig. 10. Transient response of the COI frequency in SC1, for load $\cos\phi = 1$ and load $\cos\phi = 0.8$.

the number of iterations needed is lower as the nadir was originally closer to the desired solution. Fig. 10 shows the transient response of the COI for the original case ($\cos\phi = 1$), before and after the redesign. In that figure, the results for the case of $\cos\phi = 0.8$ are also depicted. It can be seen that in both cases, the nadir after the redesign is 0.21 Hz.

4.4. Additional considerations

Some extra features may be added to the algorithm presented above. For instance, if a specific ratio between controller parameters is required, additional expressions such as (25) could be implemented. In addition to that, if a simultaneous design of nadir and ROCOF is required, (17) and (23) must be solved simultaneously. However, this objective might be difficult to achieve since these metrics might guide parameters in opposite directions. Therefore, in a case that the combined solution is not feasible, it is recommended to prioritise one of the metrics and perform the design using only that metric. To obtain better results considering only one of the metrics, additional constraints can be included as in (25).

The additional features described and the design of nadir and ROCOF simultaneously result in a system with a larger number of equations. As the number of equations increases, the problem solving may become more complex. Accordingly, it is advised to limit the number of equations by limiting the number of eigenvalues to modify. When nadir of ω_{COI} is redesigned in systems with second order dynamics, it is recommended to only modify the eigenvalue that participates the most in ω_{COI} and those with low damping. Although this may change depending on the MG and its operating point, for the variety of studied cases the algorithm found a solution to most of them. The only cases without a feasible solution were detected when an improvement of both nadir and ROCOF was performed simultaneously.

5. Experimental validation

5.1. Experimental platform

Fig. 11 shows a picture of the laboratory facilities while Fig. 12 show the implementation of this specific MG topology in the laboratory [35,36]. A 75 kVA VSC and four 15 kVA VSCs were used. One of

Fig. 11. Pictures of the laboratory facilities. (green) Centralised MG controller and measurements, (yellow) ac busbars, (violet) real-time computers, (blue) loads and (orange) power converters. (For interpretation of the references to colour in this figure legend, the reader is referred to the web version of this article.)

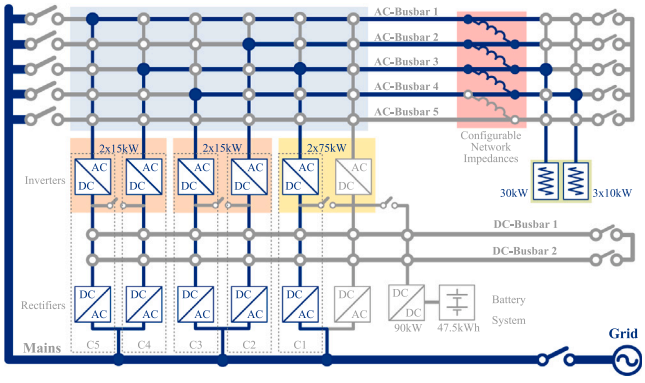

Fig. 12. Diagram of the electrical interconnections in the laboratory.

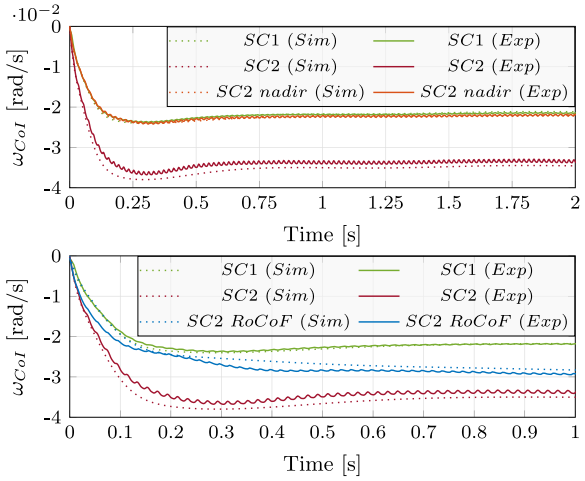

Fig. 13. Transient responses of ω_{COI} obtained from (Sim) simulations and (Exp) experiments (step variation in load L2). (green) Original scenario (*SC1*), (red) scenario with battery constraints (*SC2*), and *SC2* with (orange) nadir and (blue) ROCOF redesigns. (For interpretation of the references to colour in this figure legend, the reader is referred to the web version of this article.)

the 15 kVA VSCs was used to implement the GFL control (C4). Two programmable resistive load banks were connected at nodes B11 (L1) and B4 (L2). L2 was configured to carry out a load step of 3 kW in order to measure frequency ROCOF (at $t = 0.1$ s) and nadir. Configurable impedances were used to replicate the MG topology. A diagram of the laboratory implementation is shown in Fig. 12.

5.2. Experimental results

The analytical study was validated experimentally by performing the load steps described in Section 4.3 and then comparing experimental and analytical results of ω_{COI}. Fig. 13 shows the transient of ω_{COI} (both simulation and experimental results), for *SC1* and *SC2*, before and after the redesign for reducing (a) nadir and (b) ROCOF. The transient of ω_{COI} obtained from the tests match well with the predicted results obtained from the analytical model. Fig. 13(a) shows that after redesigning the controllers, the MG nadir for *SC2* was reduced and it reached the original value obtained in *SC1*. Then, Fig. 13(b) shows the transient response of ω_{COI}, for the case of ROCOF redesign. It can be seen that the ROCOF is reduced and it has the same value of *SC1*. The shape of the transient is not exactly the same due to the realistic elements of the experimental platform. However, these differences are relatively small.

6. Conclusion

A methodology has been proposed for continuous management of principal frequency stability parameters of a MG, namely ROCOF and nadir of frequency of centre of inertia ω_{COI}. This is achieved by applying controller parameter adjustments to the grid forming converters in the MG. For adjusting nadir, control parameters are modified by taking into consideration the parametric sensitivities of the eigenvalues that have most impact on ω_{COI}. In the case of adjusting ROCOF, control parameters are modified according to their contribution to ROCOF.

The main contribution of the paper is the proposed algorithm that ensures both stability and operational constrains are met at all times. The algorithm uses an iterative search for solution to meet the stability criteria. It has been found that parameters of droop and virtual impedance contribute most to ω_{COI} according to the parametric sensitivities. Droop parameters have the highest impact on low frequency eigenvalues and, therefore, they are mainly used to adjust both ROCOF and nadir. In addition to that, the values of virtual impedances, that are typically omitted in frequency studies, were also used to modify nadir. For the ROCOF adjustment only droop parameters were used as they are directly linked with the system frequency response and the definition of ROCOF, as considered in the literature. In comparison to previous work, parametric sensitivities were used in two ways. On the one hand, polar values of sensitivities were considered. On the other hand, they were used to move several eigenvalues at the same time. The latter prevented poorly damped eigenvalues to move to undesired locations when eigenvalues with highest impact on ω_{COI} are modified. In comparison to existing solutions, the proposed methodology is suitable for its application to any combination of GFM devices (not exclusively

VSM or droop). In addition to that, as small-signal models are obtained and updated using computational tools, no further analytical derivations are required. Another important remark is that despite the number of steps involved in the algorithm its computer implementation is rather simple. This is mostly because the algorithm mostly uses linear solver tools. Its main possible drawback is the complexity of the problem when there is a large number of restrictions applied. It is, therefore, recommendable to set the number of restrictions to minimum.

Analytical results showing the system eigenvalues and their movement during the iterative process are shown. Also, an example of parametric sensitivity is provided in order to demonstrate the parameter selection process. Finally, analytical results of the proposed methodology were validated experimentally. It was demonstrated how the nadir and the ROCOF are reestablished after a transient change of load.

In future, it would be of interest to study in detail how virtual impedance and inner primary controllers may affect frequency dynamics. This is of a particular interest for the fast frequency auxiliary services requested by grid operators. Besides, the proposed methodology can be used to adapt the dynamics of other system variables by taking into account participation factors, eigenvalues and sensitivities.

CRediT authorship contribution statement

Diana Patricia Morán-Río: Conceptualization, Methodology, Software, Validation, Formal analysis, Investigation, Writing – original draft, Visualization. **Adolfo Anta:** Conceptualization, Methodology, Resources, Writing – review & editing, Supervision, Funding acquisition. **Javier Roldán-Pérez:** Conceptualization, Methodology, Resources, Writing – review & editing, Supervision, Funding acquisition. **Milan Prodanović:** Resources, Writing – review & editing, Supervision, Funding acquisition, Project administration. **Aurelio García-Cerrada:** Resources, Writing – review & editing, Supervision, Funding acquisition, Project administration.

Declaration of competing interest

The authors declare that they have no known competing financial interests or personal relationships that could have appeared to influence the work reported in this paper.

Data availability

Data will be made available on request.

Acknowledgements

This work has been financed through Juan de la Cierva Incorporación program (IJC2019-042342-I) and project RTI2018-098865-B-C31, both from the Spanish Ministry of Science, Innovation and Universities. The work has also been financed through the research program S2018/EMT-4366 PROMINT-CAM of Madrid Government, Spain, with 50 % support of the European Social Fund. This project also received fund from the Maria the Maetzu Research program. Diana Morán is within a PhD Collaboration agreement between Comillas Pontifical University and IMDEA Energy Institute.

References

[1] Meng L, Zafar J, Khadem SK, Collinson A, Murchie KC, Coffele F, et al. Fast frequency response from energy storage systems - A review of grid standards, projects and technical issues. IEEE Trans Smart Grid 2020;11(2):1566–81.

[2] European Network of Transmission System Operators for Electricity (ENTSO-E). Need for synthetic inertia (SI) for frequency regulation. 2017, https://consultations.entsoe.eu/system-development/entso-e-connection-codes-implementation-guidance-d-3/user_uploads/igd-need-for-synthetic-inertia.pdf. (Accessed 13 January 2023).

[3] International Renewable Energy Agency (IRENA). Grid codes for renewable powered systems. 2022, https://www.irena.org/-/media/Files/IRENA/Agency/Publication/2022/Apr/IRENA_Grid_Codes_Renewable_Systems_2022.pdf. (Accessed 13 January 2023).

[4] Haberle V, Fisher MW, Prieto Araujo E, Dorfler F. Control design of dynamic virtual power plants: An adaptive divide-and-conquer approach. IEEE Trans Power Syst 2021;1. http://dx.doi.org/10.1109/TPWRS.2021.3139775.

[5] Skiparev V, Machlev R, Chowdhury NR, Levron Y, Petlenkov E, Belikov J. Virtual inertia control methods in islanded microgrids. Energies 2021;14(6):1–20. http://dx.doi.org/10.3390/en14061562.

[6] Zhong W, Chen J, Liu M, Murad MAA, Milano F. Coordinated control of virtual power plants to improve power system short-term dynamics. Energies 2021;14(4):1182.

[7] Alipoor J, Miura Y, Ise T. Stability assessment and optimization methods for microgrid with multiple VSG units. IEEE Trans Smart Grid 2018;9(2):1462–71. http://dx.doi.org/10.1109/TSG.2016.2592508.

[8] Markovic U, Chu Z, Aristidou P, Hug G. LQR-based adaptive virtual synchronous machine for power systems with high inverter penetration. IEEE Trans Sustain Energy 2019;10(3):1501–12. http://dx.doi.org/10.1109/TSTE.2018.2887147.

[9] Liu J, Miura Y, Bevrani H, Ise T. A unified modeling method of virtual synchronous generator for multi-operation-mode analyses. IEEE J Emerg Sel Top Power Electron 2021;9(2):2394–409. http://dx.doi.org/10.1109/JESTPE.2020.2970025.

[10] Chen J, Liu M, Milano F. Aggregated model of virtual power plants for transient frequency and voltage stability analysis. IEEE Trans Power Syst 2021;36(5):4366–75.

[11] González-Cajigas A, Roldán-Pérez J, Bueno EJ. Design and analysis of parallel-connected grid-forming virtual synchronous machines for island and grid-connected applications. IEEE Trans Power Electron 2022;37(5):5107–21. http://dx.doi.org/10.1109/TPEL.2021.3127463.

[12] Legry M, Dieulot J-Y, Colas F, Saudemont C, Ducarme O. Non-linear primary control mapping for droop-like behavior of microgrid systems. IEEE Trans Smart Grid 2020;11(6):4604–13. http://dx.doi.org/10.1109/TSG.2020.2998810.

[13] Barklund E, Pogaku N, Prodanovic M, Hernandez-Aramburo C, Green TC. Energy management in autonomous microgrid using stability-constrained droop control of inverters. IEEE Trans Power Electron 2008;23(5):2346–52.

[14] Wu D, Tang F, Dragicevic T, Vasquez JC, Guerrero JM, Member S. Autonomous active power control for islanded AC microgrids with photovoltaic generation and energy storage system. IEEE Trans Energy Convers 2014;1–11.

[15] Pogaku N, Prodanovic M, Green TC. Modeling, analysis and testing of autonomous operation of an inverter-based microgrid. IEEE Trans Power Electron 2007;22(2):613–25.

[16] D'Arco S, Suul JA, Fosso OB. Automatic tuning of cascaded controllers for power converters using eigenvalue parametric sensitivities. IEEE Trans Ind Appl 2015;51(2):1743–53. http://dx.doi.org/10.1109/TIA.2014.2354732.

[17] Rouco L, Pagola F. An eigenvalue sensitivity approach to location and controller design of controllable series capacitors for damping power system oscillations. IEEE Trans Power Syst 1997;12(4):1660–6. http://dx.doi.org/10.1109/59.627873.

[18] Strunz K, Abbasi E, Abbey C, Andrieu C, Annakkage U, Barsali S, et al. Benchmark systems for network integration of renewable and distributed energy resources. Tech rep, CIGRE; 2014.

[19] Morán-Río DP, Roldán-Pérez J, Prodanović M, García-Cerrada A. Influence of the phase-locked loop on the design of microgrids formed by diesel generators and grid-forming converters. IEEE Trans Power Electron 2022;37(5):5122–37. http://dx.doi.org/10.1109/TPEL.2021.3127310.

[20] Wang X, Li YW, Blaabjerg F, Loh PC. Virtual-impedance-based control for voltage-source and current-source converters. IEEE Trans Power Electron 2015;30(12):7019–37. http://dx.doi.org/10.1109/TPEL.2014.2382565.

[21] Rosso R, Wang X, Liserre M, Lu X, Engelken S. Grid-forming converters: Control approaches, grid-synchronization, and future trends—A review. IEEE Open J Ind Appl 2021;2(April):93–109. http://dx.doi.org/10.1109/ojia.2021.3074028.

[22] Zhong W, Milano F, Tzounas G. Voltage stability enhancement through active power control of converter-interfaced generation. In: 2022 IEEE PES innovative smart grid technologies - Asia. 2022, p. 550–4.

[23] Guerrero JM, García de Vicuña L, Matas J, Castilla M, Miret J. A wireless controller to enhance dynamic performance of parallel inverters in distributed generation systems. IEEE Trans Power Electron 2004;19(5):1205–13.

[24] D'Arco S, Suul JA. Equivalence of virtual synchronous machines and frequency-droops for converter-based MicroGrids. IEEE Trans Smart Grid 2014;5(1):394–5.

[25] Milano F, Ortega Á. Frequency divider. IEEE Trans Power Syst 2017;32(2):1493–501.

[26] Sauer PW, Pai MA. Power system dynamics and stability. Pearson; 1997.

[27] Ogata K. Modern contro engineering. Aeeizh; 2002.

[28] Kundur P, Balu N, Lauby M. Power system stability and control. EPRI power system engineering series, McGraw-Hill; 1994.

[29] Garofalo F, Iannelli L, Vasca F. Participation factors and their connections to residues and relative gain array. IFAC Proc Vol 2002;35(1):125–30, 15th IFAC World Congress.

[30] NERC Inverter-Based Resource Performance Task Force (IRPTF). Fast frequency response concepts and bulk power system reliability needs. Tech. rep., North American Electric Reliability Corporation (NERC); 2020.
[31] The MathWorks, Inc. Linearize simulink model at model operating point. 2022, https://es.mathworks.com/help/slcontrol/ug/linearize-simulink-model.html. (Accessed 31 May 2022).
[32] Miao B, Zane R, Maksimovic D. System identification of power converters with digital control through cross-correlation methods. IEEE Trans Power Electron 2005;20(5):1093–9. http://dx.doi.org/10.1109/TPEL.2005.854035.
[33] The MathWorks, Inc. Systems of linear equations. 2022, https://uk.mathworks.com/help/matlab/math/systems-of-linear-equations.html. (Accessed 22 August 2022).
[34] The MathWorks, Inc. mldivide Function. 2022, https://uk.mathworks.com/help/matlab/ref/mldivide.html. (Accessed 22 August 2022).
[35] Prodanovic M, Rodríguez-Cabero A, Jiménez-Carrizosa M, Roldán-Pérez J. A rapid prototyping environment for DC and AC microgrids: Smart Energy Integration Lab (SEIL). In: 2017 IEEE second int. conf. on DC microgrids. 2017, p. 421–7.
[36] Huerta F, Gruber JK, Prodanovic M, Matatagui P. Power-hardware-in-the-loop test beds: evaluation tools for grid integration of distributed energy resources. IEEE Ind Appl Mag 2016;22(2):18–26.